2011 50th IEEE Conference on Decision and Control and
European Control Conference (CDC-ECC)
Orlando, FL, USA, December 12-15, 2011

Local Stability of High Order Power Control in Cellular Networks

Benjamin C. Heinrich, University of Stuttgart
Anders Möller, Ulf T. Jönsson, Royal Institute of Technology

Abstract— **We address three major control challenges present in power control of wireless cellular networks: time-delays, interference and the binary control feedback. The power control is distributed and based on measurements of the Signal-to-Interference Ratio (SIR). This implies that the users are coupled through the mutual interference.**

In this paper we show that the interference feedback plays a fundamental role for system stability and behavior. The interference is captured by the so-called feasibility matrix, which contains the interference couplings weighted with SIR-requirements. First, we consider a simplified system and derive a Nyquist stability criterion which separates the system dynamics from the eigenvalues of the feasibility matrix. This criterion is also used to derive bounds on the rate of convergence. Second, we investigate oscillations caused by the binary feedback using harmonic balance techniques. Here, we obtain a similar separation result. Using the structure of the feasibility matrix we derive bounds on the eigenvalue location, which can be seen as a robustness result to disturbances. In an example we illustrate the stability results and predict and observe oscillation modes that are caused by the interference feedback.

I. Introduction

Power control is an important component in radio resource management of cellular networks. We consider the uplink in a CDMA (Code Division Multiple Access) cellular network. The users share spectrum, which creates interference and effects the Quality of Service (QoS) of the mobile users. The QoS is dependent on the Signal-to-Interference Ratio (SIR), which can be measured in the base station. In the uplink power control loop, the base station tracks a target SIR. Interference and radio conditions change rapidly, which means that the transmission powers of the mobiles must be updated on a fast time scale in order for the system to track the target SIR.

Due to the distributed nature of the network and constraints on the information exchange, only local measurements are used for control. Although the control algorithms are distributed, the SIR-measurements contain global information and create a nonlinear feedback between the users. The measurements are typically noisy and therefore filters are used. Filtering, control signaling and propagation introduce time-delays in the system.

There is a large literature on power control of wireless networks, see e.g [2], [4], [13], [14], to mention a few. Using different methods they consider SIR-based control algorithms. High order system models have been studied using control theoretic tools in e.g. [1], [6], [7], [8], [9], [10] and [11]. In particular, the Nyquist criterion was used in [6], but the interference feedback was not considered. The multivariate Nyquist criterion was used in [1] to prove stability of the Foschini-Miljanic algorithm for any time-delay of the interfering powers. Furthermore, in [8], the effects of binary feedback were studied using describing functions. However, the effects of interference feedback was left as an open question.

In Section II of this paper, we will use a model containing higher order dynamics and interference coupling between the users. Stability is addressed in Section III, where we will use a linearization approach to obtain local stability results for the coupled system using a Nyquist criterion. The criterion uses the eigenvalues of the feasibility matrix, similarly to how the eigenvalues of the graph Laplacian were used in [3] to prove stability of cooperative control of vehicle formations. We use structure of the feasibility matrix to obtain information of the eigenvalue location, which can be used as a robustness result.

In Section IV, we consider describing functions in a multivariate setting to predict the oscillatory behavior introduced by the binary feedback. In particular, we predict and observe oscillations due to the mutual interference that cannot be predicted by user-decoupled analysis. With interference feedback the oscillation modes often have a larger amplitude and period, which is worse from a stability perspective. The results are illustrated by a simulation in Section V.

II. System Model

We study uplink communication in a wireless cellular network where mobile stations (MS) transmit to base stations (BS). For a connection between a MS and a BS, we denote the target receiver of the transmitting mobile i by receiver i. The network model is general and may for example consist of one or several BS:s, where each BS may serve one or several MS:s.

The power control loop aims at tracking a reference QoS-value by transmitting control commands to the mobiles. The mobiles then update their transmission powers accordingly. The QoS-measure used is the SIR, denoted by $\bar{\gamma}$, and for receiver i it is given by

$$\bar{\gamma}_i \triangleq \frac{\text{signal}_i}{\text{interference}_i} = \frac{\bar{g}_{ii}\bar{p}_i}{\bar{\sigma}_i + \sum_{j\neq i}\bar{g}_{ij}\bar{p}_j}, \qquad (1)$$

where the received signal power from transmitter i is its power $\bar{p}_i$ attenuated by the channel gain $\bar{g}_{ii}$. The received interference is given by the noise level experienced at the receiver, $\bar{\sigma}_i$, and the interference from other mobiles, given by $\sum_{j\neq i}\bar{g}_{ij}\bar{p}_j$, where $\bar{g}_{ij}$ is the channel attenuation between transmitter j and receiver i.

Anders Möller is supported by the Center for Industrial and Applied Mathematics (CIAM). Ulf T. Jönsson is supported by the Swedish Research Council (VR) and the ACCESS Linnaeus Centre at KTH.

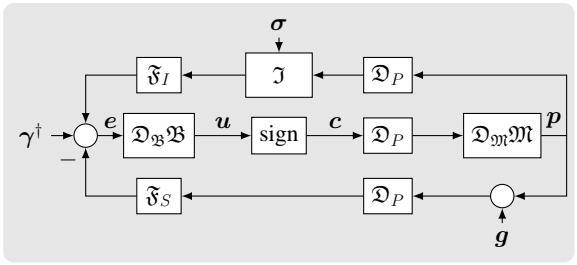

Fig. 1: Block diagram of the complete system model.

Measurements are made in logarithmic scale and we will frequently use logarithmic variables. Logarithmic variables are denoted without bar, while variables in linear scale are denoted with a bar, for example $p_i[t] = 10\log_{10}(\bar{p}_i[t])$.

The measurements of the signal and interference are noisy and filters are applied to improve performance. For user i we denote the signal filter by $\mathfrak{f}_{S,i}(q)$ and the interference filter by $\mathfrak{f}_{I,i}(q)$, where q is the time-shift operator[1] defined by $qp_i[t] = p_i[t+1]$. The SIR is computed and compared to the SIR-target, $\gamma_i^\dagger$. This gives the control error in logarithmic scale as

$$\begin{aligned} e_i[t] &\triangleq \gamma_i^\dagger - \gamma_i[t] \\ &= \gamma_i^\dagger - \mathfrak{f}_{S,i}(q)(g_{ii} + p_i[t]) + \mathfrak{f}_{I,i}(q)\mathfrak{I}_i(\boldsymbol{p}[t]), \end{aligned}$$

where $\mathfrak{I}_i(\boldsymbol{p}) = 10\log_{10}(\bar{\sigma}_i + \sum_{j\neq i}\bar{g}_{ij}\bar{p}_j) = 10\log_{10}(\bar{\mathfrak{I}}_i(\bar{\boldsymbol{p}}))$ and $\boldsymbol{p} = [p_1, \ldots, p_n]^T = 10\log_{10}(\bar{\boldsymbol{p}})$. In the BS a proper controller, $\mathfrak{b}_i(q) = \frac{b_i(q)}{a_i(q)}$ is applied, where $a_i(q)$ is a stable polynomial, i.e. all zeros lie inside the unit circle. Furthermore, we here also model $\delta_{b,i}$ delays in the BS by $q^{-\delta_{b,i}}$. A binary control command

$$c_i[t] \triangleq \text{sign}(\mathfrak{b}_i(q)q^{-\delta_{b,i}}e_i[t])$$

is then computed and transmitted to the MS.

Mobile i updates its transmission powers through a controller $\mathfrak{m}_i(q)$, which we assume to be on the form $\frac{\beta_i}{q-1}$. This implies that the power update in the mobile is causal and on the form $\bar{p}_i[t+1] = \bar{p}_i[t] + \beta_i c_i[t]$. Delays in the mobile are modeled by $q^{-\delta_m}$. Additionally, propagation delays are added to the control, signal and interference channels. A block diagram of the complete system model is shown in Figure 1, where we have used the following notation for operators

[1]The time-shift operator will be useful to write the high order difference equations that arise when delays and high order filters and controllers are modeled. We use the time-shift operator to stress the time domain interpretation. Sometimes we will instead use z, when we consider the z-transform and instead stress the frequency domain interpretation.

$\mathfrak{B} = \text{diag}(\mathfrak{b}_i)$	Base station controller
$\mathfrak{M} = \text{diag}(\mathfrak{m}_i)$	Mobile station controller
$\mathfrak{F}_I = \text{diag}(\mathfrak{f}_{I,i})$	Interference filter
$\mathfrak{F}_S = \text{diag}(\mathfrak{f}_{S,i})$	Signal filter
$\mathfrak{D}_B = \text{diag}(q^{-\delta_{b,i}})$	Delay in base station
$\mathfrak{D}_M = \text{diag}(q^{-\delta_{m,i}})$	Delay in mobile station
$\mathfrak{D}_P = \text{diag}(q^{-\delta_{p,i}})$	Propagation delay
$\mathfrak{D} = \mathfrak{D}_B \cdot \mathfrak{D}_P \cdot \mathfrak{D}_M \cdot \mathfrak{D}_P$	Total round trip delay
$= \text{diag}(q^{-\delta_i})$	
$\delta_i = \delta_{b,i} + \delta_{m,i} + 2\delta_{p,i}$	
$\mathfrak{I} = [\mathfrak{I}_1, \ldots, \mathfrak{I}_n]^T$	Interference,

where $\mathfrak{I}_i(\boldsymbol{p}) = \mathfrak{I}_i(\bar{\boldsymbol{p}}) = 10\log_{10}(\bar{\sigma}_i + \sum_{j\neq i}\bar{g}_{ij}\bar{p}_j)$. For signals we will use

$\boldsymbol{\gamma} = [\gamma_1, \ldots, \gamma_n]^T$	SIR
$\boldsymbol{\gamma}^\dagger = [\gamma_1^\dagger, \ldots, \gamma_n^\dagger]^T$	SIR-target
$\boldsymbol{p} = [p_1, \ldots, p_n]^T$	Transmission powers
$\boldsymbol{\sigma} = [\sigma_1, \ldots, \sigma_n]^T$	Receiver noise
$\boldsymbol{g} = [g_{11}, \ldots, g_{nn}]^T$	Channel attenuation
$\boldsymbol{e} = [e_1, \ldots, e_n]^T$	Control error
$\boldsymbol{c} = [c_1, \ldots, c_n]^T$	Binary control command
$\boldsymbol{u} = [u_1, \ldots, u_n]^T$	Control command.

For analysis purpose we will simplify the model by removing the sign-operator. This will be referred to as the simplified model. A similar model was derived in [6].

Consider the simplified model with $\mathfrak{B}(q) = I$, $\mathfrak{M}(q) = \frac{1}{q-1}I$ and no delays. This renders the classical Distributed Power Control (DPC) algorithm from [4], which in linear scale can be written as

$$\bar{p}_i[t+1] = \frac{\bar{\gamma}_i^\dagger}{\bar{\gamma}_i[t]}\bar{p}_i[t], \quad \forall i. \tag{2}$$

In the simplified system model, $\mathfrak{I}$ is the only nonlinear block. We will separate this nonlinear interference block from the dynamics, leading to the input-output form in Figure 2a, following the derivation in [6]. We do so by introducing the new input $\boldsymbol{\gamma}^{\dagger\dagger} \triangleq \mathfrak{F}_I^{-1}(\boldsymbol{\gamma}^\dagger - \mathfrak{F}_S\mathfrak{D}_p\boldsymbol{g})$, and pool the system dynamics into one block, H, given by

$$H \triangleq (I + \mathfrak{D}\mathfrak{M}\mathfrak{B}\mathfrak{F}_S)^{-1}\mathfrak{D}\mathfrak{M}\mathfrak{B}\mathfrak{F}_I. \tag{3}$$

We only consider decentralized algorithms using local information, which implies that all dynamics blocks are diagonal, in particular H. Assuming that the system dynamics are homogeneous we can write $H = hI$, where

$$h \triangleq \frac{\mathfrak{m}\mathfrak{b}\mathfrak{f}_I}{q^\delta + \mathfrak{m}\mathfrak{b}\mathfrak{f}_S}. \tag{4}$$

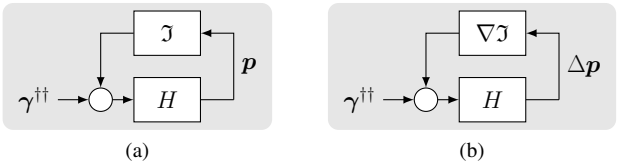

(a) (b)

Fig. 2: a) The simplified system on input-output form. b) The linearized simplified system.

III. Stability Analysis

In this section we perform a local stability analysis of the system. We start by considering the steady state of the simplified system. Then we linearize the system around the equilibrium point and perform Nyquist stability analysis.

Definition 1: Let

$$\bar{\Gamma}^{\dagger} \triangleq \text{diag}\left(\frac{\bar{\gamma}_i^{\dagger}}{\bar{g}_{ii}}\right) \quad \text{and} \quad \bar{F}_{[i,j]} \triangleq \begin{cases} 0 & \text{for } i = j \\ \bar{g}_{ij} & \text{for } i \neq j. \end{cases}$$

Then, the feasibility matrix is defined by $\bar{\Gamma}^{\dagger}\bar{F}$.
We assume $\bar{\Gamma}^{\dagger}\bar{F}$ to be irreducible, see e.g. [5].

Proposition 1: Assume that $\mathfrak{f}_I(1) = \mathfrak{f}_S(1) = 1$. Then the steady-state powers of the higher order system are the same as for the DPC-algorithm in (2). A sufficient condition for unique positive equilibrium powers is given by $\rho(\bar{\Gamma}^{\dagger}\bar{F}) < 1$, where $\rho(\cdot)$ denotes the spectral radius, and the equilibrium powers, $\bar{\boldsymbol{p}}_{ss}$, are given by

$$\bar{\boldsymbol{p}}_{ss} = (I - \bar{\Gamma}^{\dagger}\bar{F})^{-1}\bar{\Gamma}^{\dagger}\bar{\boldsymbol{\sigma}}.$$

Proof: Consider the system at steady state. We have

$$\boldsymbol{p}_{ss} = \lim_{z\to 1} \text{diag}\left(\frac{\mathfrak{m}(z)\mathfrak{b}(z)\mathfrak{f}_I(z)}{z^{\delta} + \mathfrak{m}(z)\mathfrak{b}(z)\mathfrak{f}_S(z)}\right)(\boldsymbol{\gamma}^{\dagger\dagger} + \mathfrak{I}(\boldsymbol{p}_{ss})).$$

By the integrator term and the assumption that $\mathfrak{f}_I(1) = \mathfrak{f}_S(1) = 1$ this reduces to the equation

$$\boldsymbol{p}_{ss} = \boldsymbol{\gamma}^{\dagger} - \boldsymbol{g} + \mathfrak{I}(\boldsymbol{p}_{ss}).$$

This can be written in linear scale as

$$\bar{\boldsymbol{p}}_{ss} = \bar{\Gamma}^{\dagger}(\bar{F}\bar{\boldsymbol{p}}_{ss} + \bar{\boldsymbol{\sigma}}) \quad \Leftrightarrow \quad \bar{\boldsymbol{p}}_{ss} = (I - \bar{\Gamma}^{\dagger}\bar{F})^{-1}\bar{\Gamma}^{\dagger}\bar{\boldsymbol{\sigma}}.$$

The assumption $\rho(\bar{\Gamma}^{\dagger}\bar{F}) < 1$ ensures the existence of the inverse matrix. All elements of $\bar{\Gamma}^{\dagger}$, $\bar{F}$ and $\bar{\boldsymbol{\sigma}}$ are nonnegative and, since the inverse expression can be rewritten as a convergent series expansion of $\bar{\Gamma}^{\dagger}\bar{F}$, the same condition is sufficient to guarantee nonnegative powers. ■

We now linearize the system around the equilibrium point. The linearized interference is denoted $\nabla\mathfrak{I}$ and given by

$$\nabla\mathfrak{I}_{[i,j]}(\bar{\boldsymbol{p}}_{ss}) = \begin{cases} 0 & \text{for } i = j \\ \bar{g}_{ij}\bar{p}_{j,ss}/\bar{\mathfrak{I}}_i(\bar{\boldsymbol{p}}_{ss}) & \text{for } i \neq j \end{cases}, \quad (5)$$

where $\bar{\mathfrak{I}}_i(\bar{\boldsymbol{p}}_{ss})$ is the equilibrium interference and noise. The linearized system is shown in Figure 2b.

A. Nyquist Stability Analysis

The following lemma will be useful for the stability analysis and gives intuition on how the choice of SIR-target affects stability. Let $\lambda(\cdot)$ denote the eigenvalues of a matrix.

Lemma 1: The linearized interference $\nabla\mathfrak{I}$ evaluated at $\bar{\boldsymbol{p}} = \bar{\boldsymbol{p}}_{ss}$ and the feasibility matrix $\bar{\Gamma}^{\dagger}\bar{F}$ share the same eigenvalues, i.e. $\lambda(\nabla\mathfrak{I}) = \lambda(\bar{\Gamma}^{\dagger}\bar{F})$.

Proof: Using (1) we can write

$$\bar{\mathfrak{I}}_i(\bar{\boldsymbol{p}}_{ss}) = \frac{\bar{g}_{ii}\bar{p}_{i,ss}}{\bar{\gamma}_i^{\dagger}},$$

which, plugged into (5), yields

$$\nabla\mathfrak{I}_{[i,j]}(\bar{\boldsymbol{p}}_{ss}) = \begin{cases} 0 & \text{for } i = j \\ \frac{\bar{g}_{ij}}{\bar{g}_{ii}}\frac{\bar{p}_{j,ss}}{\bar{p}_{i,ss}}\bar{\gamma}_i^{\dagger} & \text{for } i \neq j \end{cases}. \quad (6)$$

Keeping in mind that

$$\bar{\Gamma}^{\dagger}\bar{F}_{[i,j]} = \begin{cases} 0 & \text{for } i = j \\ \frac{\bar{g}_{ij}}{\bar{g}_{ii}}\bar{\gamma}_i^{\dagger} & \text{for } i \neq j, \end{cases}$$

we may rewrite (6) as

$$\nabla\mathfrak{I}(\bar{\boldsymbol{p}}_{ss}) = \text{diag}(\bar{\boldsymbol{p}}_{ss})^{-1}\bar{\Gamma}^{\dagger}\bar{F}\text{diag}(\bar{\boldsymbol{p}}_{ss}),$$

showing that $\nabla\mathfrak{I}$ is similar to $\bar{\Gamma}^{\dagger}\bar{F}$. They hence share the same eigenvalues. ■

We are now ready to state the main stability result concerning the simplified system, which separates the system dynamics from the network and SIR-target.

Theorem 1: Assume that all users have the same pooled stable transfer function $h(z)$. For $i = 1, \ldots, n$, where n is the number of users, let $\Phi\left(-\lambda_i(\bar{\Gamma}^{\dagger}\bar{F})^{-1} + h(z)\right)$ be the counter-clockwise phase rotation of $h(z)$ about $\lambda_i(\bar{\Gamma}^{\dagger}\bar{F})^{-1}$ when z sweeps the unit circle counter-clockwisely. Then the linearized system is stable if and only if

$$\sum_i \Phi\left(-\frac{1}{\lambda_i(\bar{\Gamma}^{\dagger}\bar{F})} + h(z)\right) = 0. \quad (7)$$

Since cancellations of clockwise and counter-clockwise encirclements are rare for the considered systems, we will frequently use the sufficient condition

$$\Phi\left(-\lambda_i(\bar{\Gamma}^{\dagger}\bar{F})^{-1} + h(z)\right) = 0 \qquad \forall i.$$

Proof: Starting from the determinant condition in the multivariate Nyquist criterion, we use the diagonal structure and the assumption of equal dynamics for all users to simplify the condition involving the eigenvalues of the linearized interference. Application of Lemma 1 then gives the result.

$$\begin{aligned}\Phi(\det(I - h(z)\nabla\mathfrak{I})) &= \sum_i \Phi(1 - h(z)\lambda_i(\bar{\Gamma}^{\dagger}\bar{F})) \\ &= \sum_i \Phi\left(-\frac{1}{\lambda_i(\bar{\Gamma}^{\dagger}\bar{F})} + h(z)\right)\end{aligned}$$

The system is stable if the above expression is equal to zero and hence the expression in (7) follows. ■

Consider again the DPC-algorithm in (2), where $\mathfrak{B}(z) = I$, $\mathfrak{M}(z) = \frac{1}{z-1}I$ and there are no delays. The Nyquist plot of the system dynamics block, $h(z)$, is shown in Figure 3a. The Nyquist curve is in this case the unit circle. By the Perron-Frobenius theorem for nonnegative matrices we know that the inverse eigenvalues of the feasibility matrix will lie outside the unit disc, since $|\lambda_i| < \rho(\bar{\Gamma}^{\dagger}\bar{F}) < 1, \forall i$, given that

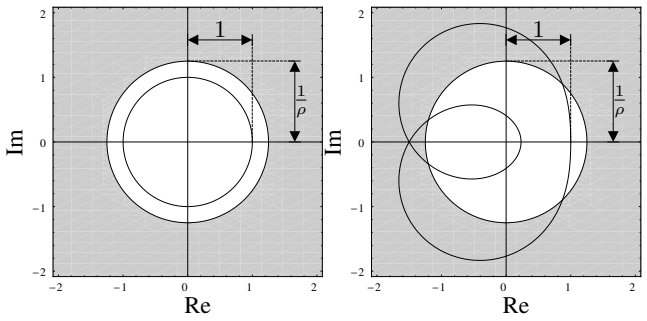

(a) $\beta = 1, \delta = 0$ (b) $\beta = 0.5, \delta = 1$

Fig. 3: Nyquist plot of the DPC- and the delayed DPC-algorithm. The inverse eigenvalues are located in the shaded region.

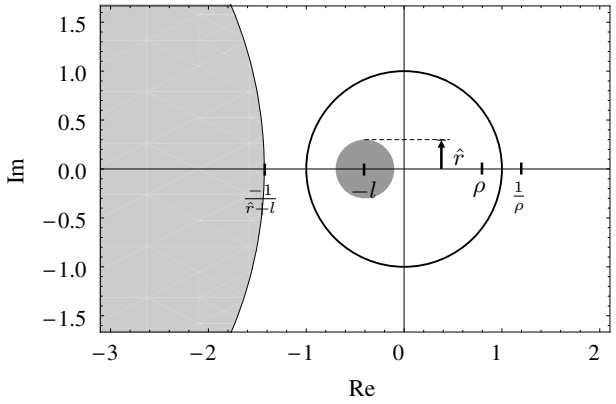

Fig. 4: Example of the locations of the eigenvalues and the inverse eigenvalues of the feasibility matrix.

the system is feasible. This verifies the well-known fact that feasibility implies stability for the DPC-algorithm.

Now consider instead the DPC-algorithm with one delay and the gain $\beta = 0.5$. The Nyquist plot of $h(z)$ is plotted in Figure 3b. We see that the Nyquist curve is not contained in the unit disc, hence, according to Theorem 1, it is necessary to check whether the curve encircles any inverse eigenvalue of the feasibility matrix. Furthermore, given that $h(z)$ has an integrator term, the Nyquist curve will cross the real axis at $z = 1$. Since for a feasible system $\frac{1}{\rho(\bar{\Gamma}^\dagger \bar{F})} > 1$, the largest eigenvalue will not influence stability. The location of the other eigenvalues is, however, critical.

B. Spectrum of the feasibility matrix

We can use more structure of the feasibility matrix to obtain more information about the location of the eigenvalues.

Definition 2: A matrix $M \in \mathbb{R}^{n\times n}$ is said to be nonnegative generalized stochastic if its elements fulfill $m_{ij} \geq 0$ and $\sum_{j=1}^{n} m_{ij} = s$, for $i = 1, \ldots, n$.

Proposition 2: Assume that $\bar{\Gamma}^\dagger \bar{F}$ is nonnegative and irreducible. Then there exist scaling multipliers $D = \text{diag}(x_i)$, where $\boldsymbol{x}$ is the positive eigenvector corresponding to $\lambda_{\max}(\bar{\Gamma}^\dagger \bar{F}) = \rho(\bar{\Gamma}^\dagger \bar{F})$, so that $M = D^{-1}\bar{\Gamma}^\dagger \bar{F} D$ is a nonnegative generalized stochastic matrix with the row sums equal to $\rho(\bar{\Gamma}^\dagger \bar{F})$.

Proof: By the Perron-Frobenius theorem the largest eigenvalue of a nonnegative irreducible matrix is positive and real. Furthermore, the corresponding eigenvector, $\boldsymbol{x}$, can be taken to be positive. We have

$$\begin{aligned} & \bar{\Gamma}^\dagger \bar{F}\boldsymbol{x} = \rho(\bar{\Gamma}^\dagger \bar{F})\boldsymbol{x} \\ \Leftrightarrow \quad & \bar{\Gamma}^\dagger \bar{F} D\mathbf{1} = \rho(\bar{\Gamma}^\dagger \bar{F}) D\mathbf{1} \\ \Leftrightarrow \quad & D^{-1}\bar{\Gamma}^\dagger \bar{F} D\mathbf{1} = \rho(\bar{\Gamma}^\dagger \bar{F})\mathbf{1}, \end{aligned}$$

where $\mathbf{1} = [1, \ldots, 1]^T$ and $D = \text{diag}(x_i)$. This proves that $M = D^{-1}\bar{\Gamma}^\dagger \bar{F} D$ is generalized stochastic with row sum $\rho(\bar{\Gamma}^\dagger \bar{F})$. ■

Proposition 3: Stability of the simplified system is equivalent to stability of the scaled system, where the block $\nabla\mathfrak{I}$ is replaced with $M = D^{-1}\bar{\Gamma}^\dagger \bar{F} D$.

Proof: We introduce scaling multipliers $D = \text{diag}(d_i)$, $d_i > 0$ into the simplified linearized system in Figure 2b, where $\hat{H} \triangleq DHD^{-1} = H$ and $\nabla\hat{\mathfrak{I}} \triangleq D^{-1}\nabla\mathfrak{I}D$. The scalings cancel in the diagonal dynamics block, but remain in the linearized interference block, $\nabla\mathfrak{I}$. Since D is non-singular, the linearized interference in the scaled variable space, $D^{-1}\nabla\mathfrak{I}D$, is similar to $\nabla\mathfrak{I}$ and hence has the same eigenvalues. Applying Lemma 1 we have that $\lambda(M) = \lambda(D^{-1}\nabla\mathfrak{I}D) = \lambda(\nabla\mathfrak{I}) = \lambda(\bar{\Gamma}^\dagger \bar{F})$. Theorem 1 then proves the statement. ■

Hence, we can without loss of generality consider nonnegative generalized stochastic matrices, $M \triangleq \bar{\Gamma}^\dagger \bar{F}$, with the spectrum $\lambda(M) = \{\rho(M), \lambda_2, \ldots, \lambda_n\}$. Note that the structure with zero-valued diagonal elements is conserved. A nonnegative generalized stochastic matrix can always be written on the form (see e.g. [12])

$$M = B + \mathbf{1}\mathbf{v}^T, \tag{8}$$

where B is a generalized stochastic matrix with row sum $r \leq \rho(M)$ and the spectrum $\lambda(B) = \{r, \lambda_2, \ldots, \lambda_n\}$, while $\mathbf{1}\mathbf{v}^T$ has spectrum $\lambda(\mathbf{1}\mathbf{v}^T) = \{\rho(M) - r, 0 \ldots, 0\}$. This implies that we can use the matrix B to obtain additional information about the spectrum of $\bar{\Gamma}^\dagger \bar{F}$. The main tool will be Gershgorin discs in combination with choice of $\mathbf{v}$.

Proposition 4: Let $\bar{\Gamma}^\dagger \bar{F}$ be nonnegative generalized stochastic with elements $m_{ij} \geq 0$, $m_{ii} = 0, \forall i$. Then $\lambda_{\max}(\bar{\Gamma}^\dagger \bar{F}) = \rho(\bar{\Gamma}^\dagger \bar{F})$, which is equal to the row sums, and the other eigenvalues are located within the disc centered around $-\frac{\rho(\bar{\Gamma}^\dagger \bar{F})}{n-1}$ with radius $\hat{r}$, given by

$$\hat{r} = \rho(|B|) \leq \min\left\{ \max_i \sum_{j\neq i} \left| m_{ij} - \frac{\rho(\bar{\Gamma}^\dagger \bar{F})}{n-1} \right|, \max_j \sum_{i\neq j} \left| m_{ij} - \frac{\rho(\bar{\Gamma}^\dagger \bar{F})}{n-1} \right| \right\},$$

where

$$B_{[i,j]} = \begin{cases} -\frac{\rho(\bar{\Gamma}^\dagger \bar{F})}{n-1} & \text{for } i = j \\ m_{ij} - \frac{\rho(\bar{\Gamma}^\dagger \bar{F})}{n-1} & \text{for } i \neq j \end{cases},$$

and where $|\cdot|$ is the componentwise absolute value.

Proof: Consider the choice $v_i = \frac{\rho(\bar{\Gamma}^\dagger \bar{F})}{n-1}, \forall i$. This gives the same center point $-\frac{\rho(\bar{\Gamma}^\dagger \bar{F})}{n-1}$ for all Gershgorin discs. The absolute row and column sums give the radius. By taking a similarity transformation using the positive eigenvector corresponding to $\rho(|B|)$, the maximum row sum will be minimized and equal to $\rho(|B|)$. ∎

Consider the following example

$$\bar{\Gamma}^\dagger \bar{F} = \tilde{M}, \quad \text{where} \quad \tilde{M}_{[ij]} \triangleq \begin{cases} 0 & \text{for } i = j, \\ l & \text{for } i \neq j. \end{cases} \tag{9}$$

The radius $\hat{r}$ from Proposition 4 is now zero, which implies that B, given in (8), has the eigenvalue $-\frac{\rho(\bar{\Gamma}^\dagger \bar{F})}{n-1}$ with multiplicity n. We have that $\rho(\bar{\Gamma}^\dagger \bar{F}) = (n-1)l$ and hence $\bar{\Gamma}^\dagger \bar{F}$ has the spectrum

$$\lambda(\bar{\Gamma}^\dagger \bar{F}) = \Big\{(n-1)l, -l, \ldots, -l\Big\}.$$

We can see that the elements l and the dimension n determines the value of $\rho(\bar{\Gamma}^\dagger \bar{F})$. Increasing l implies that the inverse eigenvalue of multiplicity $n-1$ comes closer to the Nyquist curve, which may be problematic when considering stability using Theorem 1.

Proposition 5: Any nonnegative generalized stochastic matrix with zero diagonal, $\bar{\Gamma}^\dagger \bar{F}$, can be written as the sum

$$\bar{\Gamma}^\dagger \bar{F} = \tilde{M} + \Theta,$$

where $\tilde{M}$ is given in (9) and

$$\Theta_{[i,j]} \triangleq \begin{cases} 0 & \text{for } i = j \\ \theta_{ij} & \text{for } i \neq j \end{cases},$$

where $\theta_{ij} \geq -l$ and $\sum_{j \neq i} \theta_{ij} = 0, \forall i$. Moreover, we have that $\lambda_{\max}(\bar{\Gamma}^\dagger \bar{F}) = \rho(\bar{\Gamma}^\dagger \bar{F}) = \rho(\tilde{M}) = (n-1)l$. The other eigenvalues of $\bar{\Gamma}^\dagger \bar{F}$ are located in the disc centered at $-l$ with radius $\hat{r} = \min\{\|\Theta\|_1, \|\Theta^T\|_1\}$.

Proof: To show the decomposition, choose $l = \frac{1}{n-1}\sum_{j \neq i} m_{ij}$ and $\theta_{ij} = m_{ij} - l$. Since $\bar{\Gamma}^\dagger \bar{F}$ is nonnegative generalized stochastic, the eigenvector corresponding to the largest eigenvalue is $\mathbf{1} = [1, \ldots, 1]^T$ and we have

$$\rho(\bar{\Gamma}^\dagger \bar{F})\mathbf{1} = \bar{\Gamma}^\dagger \bar{F}\mathbf{1} = (\tilde{M} + \Theta)\mathbf{1} = (n-1)l\mathbf{1}.$$

Proposition 4 states that the other eigenvalues are located in a disc centered around $-l$ with the radius

$$\begin{aligned} \hat{r} &= \min\Big\{ \max_i \sum_{j \neq i} |\theta_{ij} + l - l|, \max_j \sum_{i \neq j} |\theta_{ij} + l - l| \Big\} \\ &= \min\{\|\Theta\|_1, \|\Theta^T\|_1\} \end{aligned}$$

∎

An illustration of the location of the eigenvalues and inverse eigenvalues for an example is given in Figure 4.

IV. Describing Function Analysis

We now return to the complete system model as introduced in Figure 1. When the binary feedback is considered, the equilibrium solution is necessarily oscillating and harmonic balance techniques may be used to predict the period and amplitude. In [8] the effects of the binary control commands were investigated for interference decoupled users. However, the effect of the interference feedback was left as an open question. Under the assumption that the amplitude of the oscillation is relatively small, we may consider the linearized system as in Section III. We base our analysis on the results of [8] and extend them to the multivariate case, for which the effects of the interference can be studied.

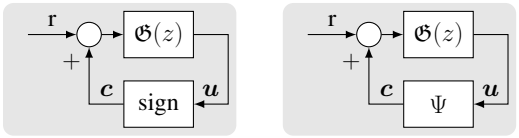

(a) (b)

Fig. 5: a) The sign-function separated from the rest of the system. b) The sign-function replaced with the describing function.

The linearized system model with the sign-function can be rewritten to the form in Figure 5a. The nonlinear sign-function is then separated from the rest of the system model, which is pooled into the new block $\mathfrak{G}$, given by

$$\mathfrak{G} \triangleq \mathfrak{D}\mathfrak{B}\mathfrak{M}(\mathfrak{F}_I \nabla \mathfrak{I} - \mathfrak{F}_S).$$

By assuming that $\mathfrak{G}(z)$ suppresses all higher order harmonics, we may use a first order harmonic balance equation to predict the limit cycle. We assume u_i to be on the form

$$u_i[t] = U_i \sin\left(\frac{2\pi}{N}(t + \phi_i)\right), \qquad i \in \{1, 2, \ldots, n\}$$

where n is the system's dimension and $N \in \mathbb{N}$ is the period length of one oscillation. The first discrete-time Fourier coefficient of $u_i[t]$ is

$$\hat{u}_i\left(j\frac{2\pi}{N}\right) = \frac{1}{N}\sum_{t=0}^{N-1} u_i[t] e^{-j\frac{2\pi}{N}t} = \frac{U_i}{2} e^{j\left(\frac{2\pi}{N}\phi_i - \frac{\pi}{2}\right)}.$$

Following the derivations of [8], the first discrete-time Fourier coefficient of the output $c_i[t]$ is given by

$$\begin{aligned} \hat{c}_i\Big(j\frac{2\pi}{N}\Big) &= \frac{1}{N}\sum_{t=0}^{N-1} \operatorname{sign}\left(U_i \sin\left(\frac{2\pi}{N}(t + \phi_i)\right)\right) e^{-j\frac{2\pi}{N}t} \\ &= \frac{1}{N}\sum_{t'=0}^{N-1} \operatorname{sign}\Big(\sin\Big(\frac{2\pi}{N}(t' + \varepsilon_i)\Big)\Big) e^{-j\frac{2\pi}{N}(t' - \lfloor\phi_i\rfloor)} \\ &= \frac{2}{N} e^{j\frac{2\pi}{N}\lfloor\phi_i\rfloor} \sum_{t'=0}^{\frac{N}{2}-1} e^{-j\frac{2\pi}{N}t'} \\ &= \frac{2}{N\sin\left(\frac{\pi}{N}\right)} e^{j\left(\frac{\pi}{N} - \frac{\pi}{2} + \frac{2\pi}{N}\lfloor\phi_i\rfloor\right)}, \end{aligned}$$

where $t' = t + \lfloor\phi_i\rfloor$, $\varepsilon_i = \phi_i - \lfloor\phi_i\rfloor$ and $\lfloor\cdot\rfloor$ is the floor function. The relation between $\lfloor\phi_i\rfloor$, ϕ_i and ε_i can be seen in Figure 6 and is due to that only $\lfloor\phi_i\rfloor$ has influence on $\operatorname{sign}(u_i[t])$ and that thus ε_i cannot be observed. Note that we have assumed N to be an even number, so that $N/2 - 1$ is an integer. Uneven period lengths in a stable oscillation

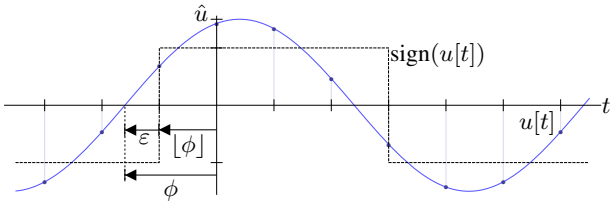

Fig. 6: Sign-function applied to a time-discrete sinus. Small changes of ε will have no effect on sign$(u[t])$.

can be viewed as alternating even periods. In Section V we will see that alternating periods can be observed.

Define $\Psi(U,N) = \text{diag}_i(\Psi_i(U_i,N))$ as the describing function, where

$$\Psi_i(U_i,N) \triangleq \frac{\hat{c}_i}{\hat{u}_i} = \frac{4}{U_i N \sin\left(\frac{\pi}{N}\right)} e^{j\left(\frac{\pi}{N} - \frac{2\pi}{N}\varepsilon_i\right)}.$$

We can now write the system as an interconnection, see Figure 5b. The first order harmonic balance equation is given by

$$\hat{\boldsymbol{u}} = \mathfrak{G}(e^{j\frac{2\pi}{N}})\hat{\boldsymbol{c}} = \mathfrak{G}(e^{j\frac{2\pi}{N}})\Psi(U,N)\hat{\boldsymbol{u}}.$$

This is equivalent to

$$(I - \mathfrak{G}(e^{j\frac{2\pi}{N}})\Psi(U,N))\hat{\boldsymbol{u}} = \boldsymbol{0},$$

where $\hat{\boldsymbol{u}} = [\hat{u}_1, \ldots, \hat{u}_n]^T$ and $\boldsymbol{0} = [0, \ldots, 0]^T$. The non-trivial solutions are hence given by

$$\det(I - \mathfrak{G}(e^{j\frac{2\pi}{N}})\Psi(U,N)) = 0.$$

Assume that $\mathfrak{F}_I = \mathfrak{F}_S = \mathfrak{F} = \text{diag}(\mathfrak{f})$. We can then write $\mathfrak{G} = \mathfrak{D}\mathfrak{B}\mathfrak{M}\mathfrak{F}(\nabla\mathfrak{I} - I) = \mathfrak{g}(\nabla\mathfrak{I} - I)$, where $\mathfrak{g} \triangleq q^{-\delta}\mathfrak{b}\mathfrak{m}\mathfrak{f}$. Now let $\Psi \triangleq \tilde{\psi}\tilde{D}$, where

$$\tilde{\psi} = \frac{4e^{j\frac{\pi}{N}}}{N\sin\left(\frac{\pi}{N}\right)}, \quad \text{and} \quad \tilde{D} = \text{diag}\left(\frac{e^{-j\frac{2\pi}{N}\varepsilon_i}}{U_i}\right).$$

The harmonic balance equation can then be written as

$$\det(I - \mathfrak{G}(e^{j\frac{2\pi}{N}})\Psi(U,N)) = \mathfrak{g}\tilde{\psi}\det\left(\frac{1}{\mathfrak{g}\tilde{\psi}}I - (\nabla\mathfrak{I} - I)\tilde{D}\right) = 0.$$

Assuming $\mathfrak{g}\tilde{\psi} \neq 0$, this is equivalent to

$$\prod_{i=1}^{n}\lambda_i\left(\frac{1}{\mathfrak{g}\tilde{\psi}}I - (\nabla\mathfrak{I} - I)\tilde{D}\right) = 0$$
$$\Leftrightarrow \quad \frac{1}{\mathfrak{g}\tilde{\psi}} - \lambda_i((\nabla\mathfrak{I} - I)\tilde{D}) = 0, \quad \text{for some } i.$$

Hence, the harmonic balance equation is fulfilled if

$$\frac{1}{\lambda_i((\nabla\mathfrak{I} - I)\tilde{D})} = \mathfrak{g}\tilde{\psi} \quad \text{for some } i. \tag{10}$$

This expression can be simplified by assuming that $U_i = U$ and $\varepsilon_i = 1/2$ for all i. We then get $\tilde{D} = \tilde{d}I$ and using

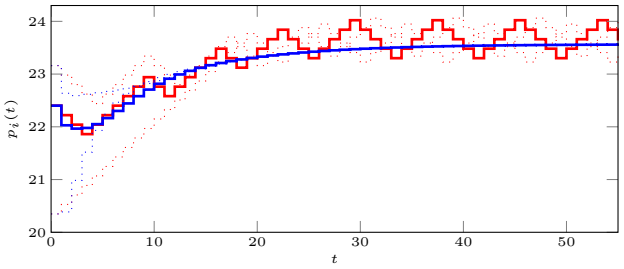

Fig. 7: Transients of the simplified system and the complete system for the example. One user of each system is highlighted, the others are dotted. We see that the simplified system converges to the equilibrium point, while the system with binary feedback converges to a limit cycle of period 8.

Lemma 1, we can rewrite (10) to

$$\frac{1}{\lambda_i(\bar{\Gamma}^\dagger\bar{F})} = \frac{\mathfrak{g}(e^{j\frac{2\pi}{N}})\psi(U,N)}{1 + \mathfrak{g}(e^{j\frac{2\pi}{N}})\psi(U,N)}, \tag{11}$$

where $\psi(U,N) \triangleq \frac{4}{UN\sin(\frac{\pi}{N})}$. Note that this has a similar structure to the Nyquist criterion in the previous section.

Since N is an integer the curve consists of discrete points and exact matching of the inverse eigenvalues only happen in special cases. It must be kept in mind that the analysis is based on approximations and when the equation is close to equality, this suggests the existence of an oscillation of the corresponding period.

Furthermore, if we find the period N, we also know the resulting amplitude of the oscillation of the transmission powers. This is because integrating the signum of a sinus function results in a triangular wave, whose amplitude is dependent on the gain β and the period length N. In the next section, we will see that the interference coupling can have a large influence on the resulting oscillations and that observed oscillations in simulations could be predicted.

V. Simulations

Consider the following example where

$$\bar{\Gamma}^\dagger\bar{F} = \begin{bmatrix} 0 & 0.01 & 0.55 \\ 0.55 & 0 & 0.01 \\ 0.01 & 0.55 & 0 \end{bmatrix},$$

and $\bar{\sigma}_i = \bar{\gamma}_i^\dagger = 10, \forall i$. Let the system dynamics be given by

$$\mathfrak{b} = 1, \quad \mathfrak{m} = \frac{0.5}{z-1}, \quad \mathfrak{f} = 1,$$

with total delay, δ, of one. Hence $h(z) = \frac{0.5}{z^2 - z + 0.5}$ and Theorem 1 is used to prove stability.

The Nyquist curve for the system is depicted in Figure 3b. The inverse eigenvalues of $\bar{\Gamma}^\dagger\bar{F}$ are $\{1.79, -0.94 \pm 1.57\}$ and we can see that the Nyquist curve does not encircle any eigenvalue. Therefore, the simplified system is locally stable. Trajectories of both the simplified and complete system model are shown in Figure 7. We see that the simplified system converges to the equilibrium point, while

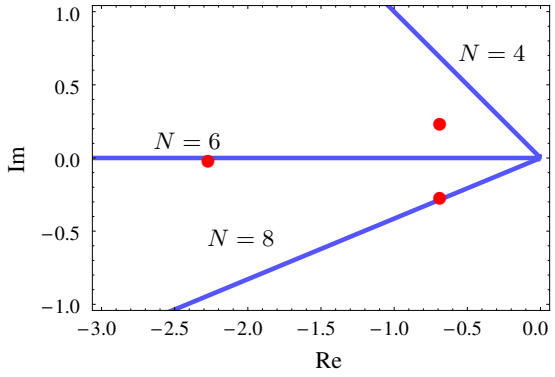

Fig. 8: Approximate harmonic balance analysis for $\delta = 1$. The points are the left-hand side of equation (10) while the lines are the right-hand side for varying U.

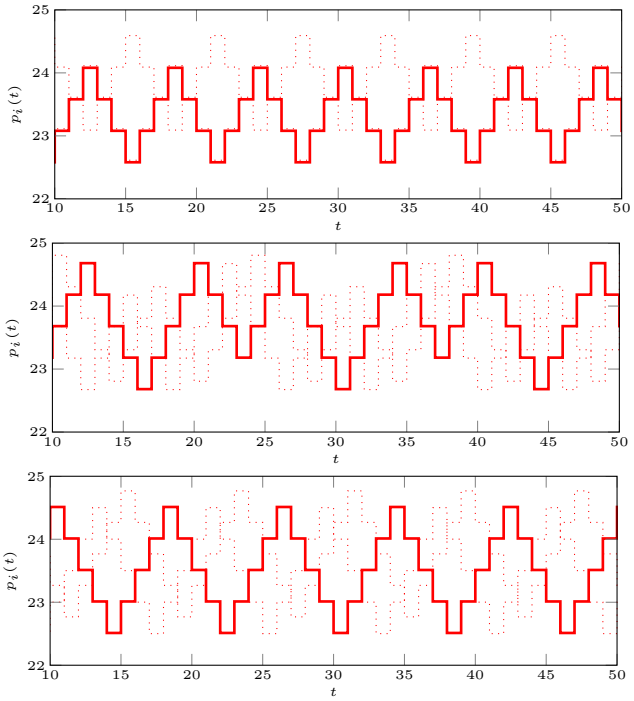

Fig. 9: Observed oscillations with periods 6,7 and 8 for $\delta = 1$. For clarity, one of the users is plotted solid.

the complete system with decision feedback converges to a limit cycle of period 8, close to the equilibrium.

The left- and right-hand sides of (10) are plotted in Figure 8 for $N = \{4, 6, 8\}$ and different values of the amplitude U. We used $\epsilon_i = 0.5$ and $U_i = U$ for all i. For this example we predict oscillations with period $N = \{6, 8\}$. Using simulations with different initial conditions, oscillation modes with $N = \{6, 7, 8\}$ are found. The observed oscillations are plotted in Figure 9.

The result of the example can be compared to the analysis in [8] where only the period $N = 6$ is predicted. This motivates taking the interference feedback into account. Another observation is that stable periods of odd length are observed. The oscillation with period $N = 7$ can be seen as alternating between a period of lenght 6 and 8. Note that this oscillation cannot be predicted using the proposed approach.

VI. Conclusions

A linearization approach is used to show that the interference feedback plays a fundamental role in stability and performance of power control in wireless networks. The eigenvalues of the linearized interference operator are equal to the eigenvalues of the feasibility matrix, containing the cross coupling gains and QoS-requirements. This is used to derive results on stability and performance through a multivariate Nyquist stability criterion that separates the system dynamics from the eigenvalues of the feasibility matrix. A robustness result to changes in the channel gains is obtained by an investigation of the location of the eigenvalues. Finally, we consider binary feedback and derive an harmonic balance equation, that also involves the eigenvalues of the feasibility matrix to predict the equilibrium oscillations that arise.

Acknowledgement: The authors are grateful to Mats Blomgren at Ericsson and Corentin Briat at KTH for valuable suggestions.

References

[1] T. Charalambous, I. Lestas, and G. Vinnicombe. On the stability of the Foschini-Miljanic algorithm with time-delays. In *Proceedings of the 47th IEEE Conference on Decision and Control*, Cancun, Mexico, 2008.

[2] M. Chiang, P. Hande, T. Lan, and C.W. Tan. Power control in wireless cellular networks. *Foundations and Trends in Communications and Information Theory*, 2(4):1–156, 2008.

[3] J.A. Fax and R.M. Murray. Information flow and cooperative control of vehicle formations. *Automatic Control, IEEE Transactions on*, 49(9):1465 – 1476, 2004.

[4] G. J. Foschini and Z. Miljanic. Distributed autonomous wireless channel assignment algorithm with power control. *IEEE Transactions on Vehicular Technology*, 44(3):420–429, 1995.

[5] F.R.Gantmacher. *The Theory of Matrices*, volume II. Chelsea Publishing Company, New York, N.Y., 1959.

[6] F. Gunnarsson. *Power Control in Cellular Radio Systems: Analysis, Design and Estimation*. PhD thesis, Linköping University, Linköping, Sweden, 2000.

[7] F. Gunnarsson and F. Gustafsson. Control theory aspects of power control in UMTS. *Control Engineering Practice*, 11(10):1113–1125, 2003.

[8] F. Gunnarsson, F. Gustafsson, and J. Blom. Dynamical effects of time delays and time delay compensation in power controlled ds-cdma. *Selected Areas in Communications, IEEE Journal on*, 19(1):141 –151, January 2001.

[9] Bore-Kuen Lee, Yuan-Ho Chen, and Bor-Sen Chen. Robust power control for cdma cellular communication systems. *Signal Processing, IEEE Transactions on*, 54(10):3947 –3956, 2006.

[10] A. Möller and U. T. Jönsson. Stability of high order distributed power control. In *Proceedings of the 48th IEEE Conference on Decision and Control*, Shanghai, China, 2009.

[11] A. Möller and U. T. Jönsson. Input output analysis of power control in wireless networks. In *Proceedings of the 49th IEEE Conference on Decision and Control*, Atlanta, USA, 2010.

[12] R. L. Soto. The inverse spectrum problem for positive generalized stochastic matrices. *Computers & Mathematics with Applications*, 43(6-7):641 – 656, 2002.

[13] N. Stefanovic and L. Pavel. A Lyapunov-Krasovskii stability analysis for game-theoretic based power control in optical links. In *Proceedings of the 48th IEEE Conference on Decision and Control*, Shanghai, China, 2009.

[14] R.D. Yates. A framework for uplink power control in cellular radio systems. *IEEE Journal on selected areas in communications*, 13(7):1341–1347, 1995.